

2018

Gulf Stream rings may rival atmospheric iron supply to the North Atlantic subtropical gyre

Tim M. Conway

Jaime B. Palter

University of Rhode Island, jpalter@uri.edu

See next page for additional authors

Follow this and additional works at: <https://digitalcommons.uri.edu/gsofacpubs>

**The University of Rhode Island Faculty have made this article openly available.
Please let us know how Open Access to this research benefits you.**

This is a pre-publication author manuscript of the final, published article.

Terms of Use

This article is made available under the terms and conditions applicable towards Open Access Policy Articles, as set forth in our [Terms of Use](#).

Citation/Publisher Attribution

Conway, T. M., Palter, J. B., & de Souza, G. F. (2018). Gulf Stream rings may rival atmospheric iron supply to the North Atlantic subtropical gyre. *Nature Geoscience*, 11(8), 594-598. doi: 10.1038/s41561-018-0162-0

Available at: <https://doi.org/10.1038/s41561-018-0162-0>

This Article is brought to you for free and open access by the Graduate School of Oceanography at DigitalCommons@URI. It has been accepted for inclusion in Graduate School of Oceanography Faculty Publications by an authorized administrator of DigitalCommons@URI. For more information, please contact digitalcommons@etal.uri.edu.

Authors

Tim M. Conway, Jaime B. Palter, and Gregory F. de Souza

Gulf Stream rings may rival atmospheric iron supply to the North Atlantic subtropical gyre

Tim M. Conway^{1,2,*}, Jaime B. Palter³ and Gregory F. de Souza²

¹ College of Marine Science and School of Geosciences, University of South Florida, St Petersburg, FL, USA

² Institute of Geochemistry and Petrology, ETH Zürich, Department of Earth Sciences, Zürich, Switzerland

³ School of Oceanography, University of Rhode Island, RI, USA.

*Corresponding author: tmconway@usf.edu; Phone: +1 727 553 3408

Keywords: GEOTRACES, biogeochemistry, nutrient supply, micronutrients, mesoscale

1 **The North Atlantic subtropical gyre is a source region of biologically-available nitrogen**
2 **to the global ocean, owing to nitrogen fixation by diazotrophic cyanobacteria¹. These**
3 **organisms have a high iron (Fe) requirement², which is typically assumed to be satisfied**
4 **in the North Atlantic by deposition of Fe-bearing Saharan dust³. However, dust supply**
5 **is episodic, resulting in highly-variable Fe concentrations at the ocean's surface^{4,5},**
6 **whilst Fe-depleted subsurface waters^{4,5} limit supply from below. Here, we report the**
7 **first observation of Fe in a Gulf Stream cold-core ring, where Fe concentrations were**
8 **elevated compared to subtropical waters, reflecting the ring's origin in the Fe-rich Slope**
9 **Sea. Using surrounding data from the GEOTRACES GA03 section and recent advances**
10 **in satellite tracking of rings, we calculate that cold-core rings provide a net flux of**
11 **$0.3 \pm 0.17 \times 10^8$ mol Fe yr⁻¹ across the north-western gyre edge, within the wide range of**
12 **estimates of atmospheric Fe supply over the entire gyre area, 0.4 - 8.6×10^8 mol Fe yr⁻¹**
13 **(median 2×10^8 mol Fe yr⁻¹). By linking mesoscale ocean circulation to Fe supply, our**
14 **results provide a new view of subtropical Fe dynamics that challenges the paradigm**
15 **that atmospheric deposition persistently dominates subtropical North Atlantic iron**
16 **supply.**

17

18 *Iron sources to the North Atlantic subtropical gyre.* Primary productivity in much of the
19 Southern Ocean as well as the equatorial and sub-Arctic Pacific has been shown to be limited
20 by iron (Fe)^{6,7}. In contrast, in oligotrophic regions of the ocean such as the North Atlantic
21 subtropical gyre (NASG), productivity is thought to be limited instead by macronutrients, and
22 thus much less sensitive to Fe addition^{7,8}. Owing to its proximity to the Sahara Desert, the
23 North Atlantic receives the largest atmospheric dust fluxes globally³, resulting in dissolved
24 Fe concentrations of up to 2 nmol kg⁻¹ in surface waters⁵. It has thus long been assumed that
25 dust provides ample Fe for phytoplankton to utilise available macronutrients in this region.

26 However, the degree to which Fe from dust dissolves in seawater and is stabilised therein by
27 organic ligands is widely debated⁹. Moreover, dust deposition is highly localised and
28 episodic, varying dramatically with storm activity, location and season^{3,5,10}, and may quickly
29 overwhelm the capacity of seawater and organic ligands to maintain the supplied Fe in
30 solution, leading to precipitation. In fact, dissolved Fe concentrations at the surface in the
31 western gyre can be as low as 0.09 nmol kg⁻¹ during winter, with a potentially growth-
32 limiting dissolved Fe minimum (0.02-0.20 nmol kg⁻¹) present in subsurface waters (50-150
33 m) year-round^{4,5}. Background Fe concentrations of the gyre in the absence of dust deposition
34 are also reproducibly low (Suppl. Info.). In addition to limiting nitrogen uptake in the North
35 Atlantic¹¹, a recent study has found that Fe may also limit phosphate acquisition by the
36 microbial community in the North Atlantic in areas distal from the Saharan dust plume¹².
37 Therefore, all sources of Fe must be considered for their potential to fuel primary
38 productivity within the gyre.

39

40 ***Gulf Stream rings.*** As early as the 1930s, scientists discovered boluses of anomalously cold
41 water in the NASG and inferred that eddies must transport water from the Slope Sea, which
42 lies between the continental shelf and the Gulf Stream, into the gyre¹³. These ‘cold-core
43 rings’ are formed when a Gulf Stream meander becomes so large that it folds back onto itself,
44 forming a loop that pinches off from the main current. These rings trap Slope Sea water, and
45 are easily identifiable in satellite observations as they propagate into the subtropical gyre,
46 characterised by a circular depression of sea-surface height. Although it has been proposed
47 that eddy-driven, cross-Gulf Stream transport constitutes an important supply of phosphorus
48 (P) to the subtropical gyre¹⁴, and it is well known that lateral processes in general play a role
49 in supplying macronutrients to the gyres¹⁵⁻¹⁸, the effect of Gulf Stream rings on Fe transport
50 has not been considered, largely due to a paucity of high-quality Fe data. Here, by combining

51 a recent satellite-derived dataset of mesoscale eddy activity¹⁹ with a new dissolved Fe
52 dataset⁴ from a North Atlantic GEOTRACES section^{20,21} (GA03; Fig. 1), we quantify the
53 potential of Gulf Stream rings to supply Fe to the NASG. The GA03 dataset is ideal for this
54 purpose, with two stations located in the Slope Sea, several within the NASG, and one station
55 (USGT11-6) serendipitously situated at the edge of a Gulf Stream cold-core ring (Fig. 1).

56

57 ***Cross Gulf Stream iron transport.*** Slope Water is identifiable in the GA03 section by its low
58 temperature and salinity (Figs 2-3), and is characterised by high concentrations of
59 macronutrients²¹ and CFCs²⁰, reflecting upwelling of nutrient-rich water and contributions
60 from shelf and Labrador Sea Water sources^{21,22}. Slope Water is also greatly enriched in
61 dissolved Fe compared to waters of equivalent density in the subtropical gyre⁴ (Fig. 3; 0.64
62 vs. 0.30 nmol kg⁻¹ above the 1026.5 isopycnal; Methods). These higher Fe concentrations
63 have been attributed to a margin sediment source, which is important throughout the mid-
64 depth (~600-2000 m) subtropical North Atlantic⁴. Within the subtropical gyre, however, a
65 wedge of Fe-depleted Subtropical Mode Water (STMW)²³ separates this enriched mid-depth
66 layer from the surface (Fig. 2). The cold-core ring sampled along GA03 transports Slope Sea
67 water into the Fe-depleted gyre, with dissolved Fe concentrations 25% higher above the
68 1026.5 isopycnal, and 60% higher above 500 m, than the open gyre (Figs 2-3).

69 The observation of a ring of Fe-rich Slope Water within the Fe-poor subtropical gyre
70 suggests that rings could represent a significant source of Fe to the NASG, assuming the
71 GA03 observations of the difference between gyre and Slope Sea Fe concentrations are
72 characteristic for the region. Such an assumption is justified for a number of reasons, as
73 discussed here and in more detail in the Supplementary Information. Firstly, the Fe-poor
74 nature of the NASG waters is well documented; not only do the US GEOTRACES GA03
75 zonal section⁴ (2011) and the separate Dutch GEOTRACES GA02 meridional transect²⁴

76 (2010) both show consistently low Fe concentrations through waters of the subtropical gyre,
77 but three station reoccupations near Bermuda also provide evidence for the temporal stability
78 of low Fe concentrations in the NASG over a period of three years^{25,26}. The temporal
79 variability of Slope Sea Fe concentration cannot be similarly directly assessed since the Fe
80 concentration of its subsurface waters has not been previously reported. However, the
81 propagation of characteristic sediment-derived Fe stable isotope compositions into the ocean
82 interior⁴ suggests that the Slope Sea Fe is relatively long-lived, consistent with the
83 observation here of elevated Fe within a ring that was shed a number of weeks before
84 sampling (Fig. 2). Furthermore, earlier work describes a qualitatively similar gradient of high
85 Fe in very surface North American shelf waters decreasing into the open gyre²⁷. At the basin
86 scale, water column Fe datasets from reoccupied ocean stations in three other regions of the
87 ocean, both with and without proximal sediment sources, also indicate the relative temporal
88 stability of Fe profiles, similar to the macronutrients, at least on a sub-decadal
89 timescale^{20,26,28}. We thus feel confident in using the GA03 Fe data as sufficiently
90 representative of the system in order to calculate the contribution of ring-driven transport to
91 the Fe budget of the gyre.

92 This ring-driven Fe transport flux depends on: 1) the number of rings that cross the
93 Gulf Stream per year, 2) the amount of dissolved Fe each ring carries, and 3) the fraction of
94 this transported Fe that remains within the gyre rather than being re-entrained into the Gulf
95 Stream. Recent progress in detecting and tracking eddies^{19,20} makes the quantification of the
96 ring-driven flux timely. We identified all Gulf-Stream-crossing cold-core rings in a
97 database¹⁹ of eddies detected in satellite altimetry data for 1993-2014 (Methods), and
98 calculate that an average of 7.7 ± 2.5 cyclonic rings cross the Gulf Stream each year (Suppl.
99 Fig. 1), with an average surface area of $3.9 \pm 1.5 \times 10^4$ km² (the equivalent of a circular vortex,
100 radius 111 ± 70 km). As the ring identified at station USGT11-6 was shed many weeks before

101 sampling (Methods) and its Fe inventory may thus have been affected by uptake, scavenging,
102 or physical mixing of Fe, we chose not to use this ring as the endmember in our calculations.
103 Instead, since cold-core rings enclose Slope Sea water pinched off by the Gulf Stream, we
104 assumed that the average Fe concentration in Slope Water above the 1026.5 isopycnal
105 (0.64 ± 0.12 nmol kg⁻¹; stations USGT11-1 and 11-2) is representative of the initial dissolved
106 Fe concentration in the core of the average cold core ring. We consider the water column
107 above the 1026.5 isopycnal since we are interested in Fe that is accessible to NASG surface
108 ecosystems over the annual cycle, and this isopycnal represents the density of the maximum
109 NASG winter mixed layer.

110 If all rings dissipate entirely within the gyre, as assumed in an early study²⁹, their
111 near-surface Fe burden would ultimately enter the subtropical mixed layer. In this view, the
112 volume flux due to rings entering the gyre is balanced by an equivalent volume transport out
113 of the gyre, largely due to warm-core rings, with the average Fe concentration of the interior
114 gyre above the 1026.5 isopycnal (0.30 ± 0.10 nmol kg⁻¹). Given the 0.34 nmol kg⁻¹ Fe
115 concentration difference and the ring statistics from satellite altimetry, the assumption of
116 complete dissipation leads to a ring-driven Fe supply to the subtropical gyre of $0.3 \pm 0.17 \times 10^8$
117 mol dissolved Fe yr⁻¹, accompanied by a dissolved phosphate supply of $1.3 \pm 0.8 \times 10^{10}$ mol
118 year⁻¹; Methods).

119 Our estimate of the ring-driven Fe and phosphate supply may be considered an upper
120 limit, given that rings can be re-entrained into the Gulf Stream after only partial dissipation³⁰.
121 In these cases, only a fraction of the nutrients within the ring may be biologically consumed
122 within the ring and/or mixed laterally with surrounding subtropical waters, before being re-
123 entrained. A conservative estimate for the ring-driven nutrient supply is provided by
124 assuming that nutrients become available only after physical dissipation of the rings, which
125 assumes no biological consumption in the ring before re-entrainment. Assuming a lateral

126 diffusivity of $300 \text{ m}^2 \text{ s}^{-1}$, as diagnosed from float observations of analogous cold-core rings
127 shed from the Kuroshio Extension³⁰, half of the volume-integrated Fe anomaly in the ring
128 would be mixed with surrounding waters within two months, and $\leq 15\%$ of the integrated Fe
129 would remain at the end of one year (Methods; ED Fig. 2). With ring lifetimes thought to
130 average more than a year³¹, we estimate that accounting for re-entrainment of rings into the
131 Gulf Stream after only partial dissipation would reduce our estimate by 15% at most.
132 Additionally, rings are not the only processes that can transport Fe and nutrients across the
133 Gulf Stream. Rather, a suite of mesoscale processes, including but not limited to rings, can
134 mix nutrients down-gradient from the relatively high concentrations of the Slope Water into
135 the NASG. We estimate that the total Fe supply due to down-gradient mixing across the Gulf
136 Stream may be up to seven times larger than our ring-derived estimates (Methods).

137

138 ***Comparison of ring-derived fluxes with atmospheric supply.*** How does the ring-driven flux
139 of soluble Fe to the NASG compare to that delivered by atmospheric deposition? Answering
140 this question requires a robust quantification of atmospheric Fe fluxes, which are highly
141 uncertain. Drawing upon a wide variety of independent observation- and model-based
142 estimates, we have established a representative range of gyre-wide atmospheric Fe deposition
143 fluxes to the NASG (Methods; Suppl. Info). A key uncertainty for the biogeochemical
144 relevance of atmospheric Fe deposition is the solubility of the Fe delivered to the surface
145 ocean. Different studies approach this question differently. For example, some models
146 included in our compilation include Fe as a prognostic variable and directly simulated its
147 solubility; in these, Fe solubility in the dust deposited to the NASG ranged between $\sim 1\text{-}2\%$
148 (Table S1). In other studies, where only total Fe deposition was reported, we calculated
149 soluble Fe delivery by assuming an appropriate upper bound of 5% solubility (see a more
150 detailed discussion in Supplementary Information). The resulting range of atmospheric

151 soluble Fe fluxes over the entire area of the subtropical gyre spans a factor of more than 20,
152 from $0.4\text{--}8.6\times 10^8$ mol Fe yr⁻¹ (Fig. 4), with a median of 2×10^8 mol Fe yr⁻¹. Our estimate of
153 ring-driven soluble Fe transport across one boundary of the NASG thus represents between
154 3% and 75% of the range of estimated atmospheric deposition fluxes over the entire gyre
155 surface, or 15% of the median deposition flux (Fig 4). In the face of the uncertainty of the
156 magnitude of atmospheric soluble Fe supply, this result indicates that ring-driven transport of
157 Fe across the Gulf Stream is quantitatively important for Fe supply to the gyre. This is
158 especially true for the north-western gyre, since the westward propagation of the rings means
159 that they are most likely to dissipate within the north-western gyre. A scale analysis suggests
160 that this ring-driven supply of Fe may in fact be the dominant mechanism of Fe supply to this
161 region if the rings dissipate within ~1000 km of the Gulf Stream (Fig. 4). Such a significant
162 role for ocean circulation in Fe supply via lateral transport represents a paradigm shift in our
163 understanding of sources of Fe to the subtropics, and parallels recognition of the importance
164 of lateral transport for macronutrient budgets of subtropical gyres^{15,18}. Our quantification of
165 the ring-driven Fe flux suggests that such transport processes must be included in Fe budgets
166 and models of ocean biogeochemistry.

167

168 ***Implications for gyre biogeochemistry.*** Two other factors combine to reinforce the
169 importance of cross-Gulf Stream Fe transport for the subtropical Fe budget and the
170 biogeochemistry of the NASG. First, Slope Water contains a higher excess of Fe-binding
171 ligands than the open surface gyre³². Not only does this mean that a higher percentage of the
172 dissolved Fe coming from the Slope Sea may be bioavailable compared to dust-derived Fe,
173 but a supply of excess ligands could also enhance *in situ* Fe dissolution from dust as well as
174 stabilising the Fe thus released³³. Second, ring-driven Fe supply is accompanied by a supply
175 of the macronutrients nitrate and phosphate to the gyre, and, importantly, as previously

176 noted¹⁴, by an excess supply of phosphate relative to nitrate (Fig. 2d; Methods). If rings also
177 carry an excess of Fe over nitrate relative to the physiological requirements of non-
178 diazotrophic phytoplankton, this could create an ecological niche for diazotrophs³⁴.
179 Resource-competition theory³⁵ suggests that in order for ring-driven transport to support
180 diazotrophy in the NASG, the supply of Fe and P relative to N should exceed their relative
181 requirement by non-diazotrophic phytoplankton³¹.

182 Here, our calculations yield a PO₄:NO₃ ratio of ring-driven transport below 1:15, i.e.
183 an excess of PO₄ relative to the Redfield ratio of 1:16, consistent with previous results
184 suggesting excess PO₄ supply to the NASG^{14,36}. Therefore, the surplus PO₄ in rings should
185 become available to diazotrophs following exhaustion of the NO₃ supply by non-
186 diazotrophs. The corresponding Fe:NO₃ ratio in the rings is ~1:8800, or 0.11 mmol mol⁻¹.
187 Cell quota studies³⁷ suggests that non-diazotrophic phytoplankton cells have Fe:N ratios of
188 0.06-0.31 mmol mol⁻¹ N (reported Fe:PO₄ ratios of 1-5 mmol mol⁻¹, and converted assuming
189 a Redfield N:P ratio). If the non-diazotrophic assemblage is comprised of cells at the low-
190 end of this range, then the ring-driven nutrient supply could support diazotrophy. Otherwise,
191 rings would be expected to leave surplus PO₄, but little Fe, behind after non-diazotrophic
192 exhaustion of NO₃, priming the system for N₂ fixation in response to atmospheric Fe
193 deposition events.

194 We thus speculate that, dependent on the microbial and phytoplankton assemblage,
195 and together with the stabilizing and solubilizing effect discussed above, ring-driven Fe
196 supply may contribute to the support of diazotrophy in the NASG, whilst also potentially
197 influencing P acquisition¹². Even if ring transport of Fe does not support diazotrophy directly,
198 ring transport of excess phosphate would still be expected to support diazotrophy in response
199 to atmospheric Fe deposition events. More broadly, eddy-driven transport of Fe may be
200 important in other similarly dynamic regions of the oceans, including the South Atlantic,

201 where Agulhas rings carry elevated Fe concentrations into the subtropics²⁶, and the North
202 Pacific, where Haida eddies carry Fe from Alaskan shelf waters to the Fe-limited open
203 ocean³⁸. Patchy supply of Fe and macronutrients by eddies may thus have a significant effect
204 on local and regional biogeochemistry, playing an important and often-overlooked role in
205 primary productivity, nitrogen fixation and carbon cycling within oligotrophic gyres.

206

207 **Methods**

208

209 **Data availability.** GA03 dissolved Fe concentration data shown in Figs. 2-3 and used in
210 calculations are taken from Conway and John⁴. Supporting data for macronutrients, salinity
211 and temperature along GA03 are reproduced from the Ocean Data Facility²¹ and all GA03
212 data are freely available²⁰ in the GEOTRACES Intermediate Data Product 2014.

213

214 **Satellite-derived eddy database.** Faghmous *et al.*¹⁹ provide a database of eddies detected in
215 satellite altimetry, compiled for the years 1993-2014. In this database, a cyclonic eddy is
216 defined as the outermost closed contour of altimetric sea level anomaly (SLA) containing a
217 single minimum in sea level. This minimum is defined as a grid cell whose SLA is less than
218 its surrounding 24 neighbouring grid points (on a 5×5 grid), where each side of a grid box is
219 0.25° in latitude or longitude. To track the eddies over time, all eddies in the next day SLA
220 image within a geographical boundary are checked to see whether there is an eddy that
221 qualifies to be stitched to the current day's eddy to form a track. This geographical boundary
222 accounts for westward propagation at the Rossby phase speed.

223

224 **Cross-Gulf Stream ring identification.** Using the Faghmous *et al.*¹⁹ database, we identified
225 and recorded the size of cold-core rings that cross the climatological Gulf Stream position

226 into the subtropical gyre as follows: 1) Construct a monthly climatology of sea surface height
227 (SSH) over the satellite record; 2) Interpolate the monthly mean climatological SSH along
228 each cyclonic eddy track in the vicinity of the Gulf Stream; 3) Tag any eddies that cross from
229 north of the climatological Gulf Stream position (regions with SSH below 0.52 m from the
230 AVISO absolute dynamic topography) to the subtropical side of the Gulf Stream (SSH
231 greater than 0.55 m) and persist as a coherent track for at least three weeks.

232 We compared the performance of this objective identification against an ad-hoc visual
233 assessment for a random subset of the satellite record (comprising 8 years and 66 eddies –
234 more than a third of all cold-core rings from the final record). For two examples of this ad-
235 hoc visual assessment, see Suppl. Animation 1 for a clear example of a cold core ring
236 penetrating into the subtropical gyre from 1993, and Suppl. Animation 2 for the ring sampled
237 at station USGT11-6 from 2011. The eddies identified by the algorithm generally have the
238 expected characteristics of a cold-core ring: they are formed from a steep meander of the Gulf
239 Stream, shed to the south, and propagate westward. Moreover, the eddy amplitude (i.e. the
240 absolute value of the sea level anomaly along the track) is 46 cm, further verifying that these
241 rings travel across the position of the climatological Gulf Stream and are, thus, large negative
242 anomalies relative to the average subtropical sea-surface height. Furthermore, our estimate of
243 ring number, 7.7 ± 2.5 rings yr^{-1} (Suppl. Fig. 1), is within the uncertainty bounds of earlier
244 work that counted the number of rings identified by cold anomalies in satellite sea surface
245 temperature snapshots and divided by an estimate of their lifetime³⁹.

246

247 ***Estimation of dissolved Fe anomaly in a ring.*** We estimated the dissolved Fe concentration
248 within a cold-core ring based on the Slope Sea stations from the GA03 Section dataset⁴. To
249 do this, we calculated the depth integrated average Fe concentration observed in near-surface
250 layers (i.e. in and above the density of the STMW, isopycnal 1026.5). The 1026.5 isopycnal

251 was at depths of ~100 m in the Slope Sea, deepening to 350 m in the open gyre (Fig. 2), and
252 is taken as the deepest relevant depth of Fe that may become available for productivity in the
253 gyre, since this isopycnal represents the maximum winter mixed layer density in the gyre⁴⁰.
254 Taking data from 0-100 m at stations USGT11-1 and -2 within the Slope Sea gave an average
255 of 0.64 nmol kg⁻¹ for the Slope Sea, with a standard deviation of 0.12 nmol kg⁻¹. Similarly,
256 taking the mean of data from 0 to 350 m at GA03 stations USGT11-8 and USGT11-10, to
257 represent the interior of the gyre, gave 0.30 nmol kg⁻¹, with a standard deviation of 0.10 nmol
258 kg⁻¹. We excluded the outlier top data point at Station 8 (1.2 nmol kg⁻¹) from the average to
259 preclude any effect from recent dust deposition or contamination biasing the gyre average.
260 The calculated Fe anomaly (ΔFe) within an average cold-core ring is thus assumed to be the
261 difference between these numbers (0.34 nmol kg⁻¹). We chose not to use the average
262 observed ring concentrations from above the 1026.5 isopycnal or above 500 m at USGT11-6
263 (0.37 and 0.47 nmol kg⁻¹ respectively) as the Slope Water end member, because it is clear
264 from SSH data that (a) station USGT11-6 was at the edge of the ring and (b) the ring was
265 shed about 5–6 weeks before sampling, and thus has presumably lost significant Fe due to
266 scavenging, biological uptake, and mixing with subtropical waters, as suggested by the strong
267 interleaving seen in Fig. 3 (Fe dissipation estimate below).

268

269 ***Calculation of ring-driven Fe transport.*** We calculated the total ring-driven supply of Fe to
270 the NASG (φ_{Fe}) as the product of the Fe anomaly in a ring relative to subtropical
271 concentrations (ΔFe) times the number of rings (n), their surface area (A), and a characteristic
272 depth scale of the Fe anomaly accessible to the surface ocean over a seasonal cycle (D):

273
$$\varphi_{\text{Fe}} = \Delta\text{Fe} \times n \times A \times D \quad (1)$$

274 where $\Delta\text{Fe} = 0.34 \mu\text{mol m}^{-3}$ (equivalent to 0.34 nmol kg⁻¹), $n = 7.7 \text{ rings yr}^{-1}$, $A = 3.9 \times 10^4$
275 km², and $D = 225$, which is the average depth of the 1026.5 isopycnal across the Slope Sea

276 and subtropical gyre stations. Under these assumptions, the total ring-driven supply of Fe is
 277 equal to $0.3 \pm 0.17 \times 10^8$ mol dissolved Fe year⁻¹. The uncertainty is propagated from the
 278 standard deviations of the ring number (7.7 ± 2.5 per year), size ($3.9 \pm 1.5 \times 10^4$ km²), and Fe
 279 concentrations ($0.2 \mu\text{mol m}^{-3}$), and includes an estimate of uncertainty on D of 50 m. This
 280 calculation makes the implicit assumption that the volume transport by cold core rings into
 281 the subtropical gyre (represented by $n \times A \times D$) is balanced by an equal volume transport
 282 out of the subtropical gyre with Fe concentrations equal to those observed in the GA03
 283 subtropical stations.

284

285 ***Estimation of the Fe dissipation from the ring.*** To estimate the amount of Fe that would
 286 dissipate from a cold-core ring during its time in the gyre, we use the same diffusivity as was
 287 observed for cold-core rings shed from the Kuroshio Extension³⁰. We assume a circular
 288 vortex³⁰ with initial tracer concentration:

$$289 \quad \text{Fe}(r, 0) = \text{Fe}_o + \text{Fe}_1 \exp\left(\frac{-r^2}{a^2}\right) \quad (2)$$

290 where Fe_o is the subtropical Fe concentration, taken to be $0.30 \mu\text{mol m}^{-3}$; (equivalent to 0.30
 291 nmol kg^{-1}); Fe_1 is the Fe anomaly at the centre of the ring relative to the background
 292 concentration, set at $0.34 \mu\text{mol m}^{-3}$ (equivalent to 0.34nmol kg^{-1}); r is the distance from the
 293 ring's centre; and a^2 sets the exponential decay length scale, taken to be 48 km, as was found
 294 to be appropriate for a ring of about 100 km radius by Qiu and colleagues³⁰. The isopycnal
 295 diffusion of Fe out of the ring proceeds according to:

$$296 \quad \frac{\partial \text{Fe}(r,t)}{\partial t} = A_h \frac{1}{r} \frac{\partial}{\partial r} \left[r \frac{\partial \text{Fe}(r,t)}{\partial r} \right] \quad (3)$$

297 where A_h is the diffusivity, taken to be equal to $300 \text{ m}^2 \text{ s}^{-1}$ as found for the cold-core rings
 298 shed from the Kuroshio³⁰. Suppl. Fig. 2a. shows the solution to this equation at various
 299 times, and illustrates the rapid loss of Fe from the ring core. Suppl. Fig. 2b quantifies the

300 integrated Fe anomaly in the central 50 km of the ring (relative to the background subtropical
301 concentration) as a function of time. These results show that after only 2 months, the ring
302 would lose half of its integrated Fe anomaly, with less than 15% remaining after 1 year.
303 These timescale calculations are consistent with the observation of strong interleaving within
304 the ring in the GA03 section (Fig. 3), which satellite data suggest was shed from the Gulf
305 Stream 5–6 weeks before it was sampled.

306

307 ***Comparison of ring-driven flux to scaling for total down-gradient mixing of Fe and other***

308 ***terms in the Fe conservation equation.*** A basic scale analysis of the down-gradient transport

309 of Fe provides a check on the order of magnitude of the ring-based estimate. Such along-

310 isopycnal diffusion scales as $\frac{A_h D \Delta \text{Fe}}{L^2}$, where A_h is the isopycnal diffusivity, with estimates of

311 A_h ranging from 500 to 1500 m² s⁻¹; D is the thickness of the vertical layer of interest

312 (nominally the 225 m average depth of the 26.5 isopycnal⁴⁰); ΔFe is the difference in Fe

313 concentrations across the Gulf Stream of 0.34 nmol kg⁻¹; and L is the horizontal length scale

314 over which the Fe change is observed (i.e. about 50 km). We note that these diffusivity

315 estimates for A_h may be higher than that used to estimate the mixing out of the rings above, as

316 turbulent diffusivity scales with the length over which the turbulent motions are averaged⁴¹.

317 With these parameter choices, the down-gradient diffusion of Fe into the subtropical gyre is

318 estimated as supplying 480-1450 μmol m⁻² year⁻¹, with the range coming from the range of A_h

319 values (500 to 1500 m² s⁻¹). For a Gulf Stream length along the Slope Sea of 2000 km and

320 over a 50 km width, the total supply of Fe due to down-gradient diffusion is estimated at

321 between 0.3×10⁸ and 2×10⁸ mol year⁻¹. This calculation yields a flux that is up to 7 times

322 larger than the ring-derived estimate. We take the agreement in order of magnitude between

323 the low end of this estimate with that derived from the ring statistics as an indication that the

324 ring-based estimate of Fe supply is within reasonable limits. That the diffusion-based

325 estimate may be substantially larger than the ring-based estimate is consistent with the idea
326 that rings are one of many mesoscale processes moving Fe from the Slope Sea across the
327 Gulf Stream.

328 This isopycnal mixing term is one of several physical mechanisms that can potentially
329 transport Fe into or out of the subtropical gyre, in the layer above the annual maximum mixed
330 layer. Following the approach in Williams and Follows¹⁵, we provide a scale analysis of the
331 following additional transport terms for comparison to the ring-driven transport. On a
332 seasonal basis, the vertical entrainment term may dominate phosphate and nitrate budgets¹⁵,
333 since there is an accumulation of these macronutrients in the seasonal pycnocline. However,
334 iron is depleted to depths below even the permanent pycnocline (i.e. below the 26.5
335 isopycnal). Thus, we expect vertical entrainment to be a small term, and may cause dilution
336 of the iron deposited on the ocean surface through a deepening mixed layer. In any case, for
337 an iron budget integrated to the base of the deepest annual mixed layer, the vertical
338 entrainment term is approximately offset by the biological export term¹⁵, and we expect the
339 budget to be dominated by Ekman advection, diapycnal mixing, and vertical advection, each
340 of which is scaled in the following analysis.

341 Ekman advection is estimated from the average down-front winds along the Gulf
342 Stream create, which create Ekman transports of $U = 2 \text{ m}^2 \text{ s}^{-1}$ (equivalent to 4 cm s^{-1} over an
343 Ekman layer of 50 m depth¹⁴) acting across surface Fe concentrations that decrease from 0.6
344 to $0.3 \mu\text{mol m}^{-3}$ going southward across the Gulf Stream. Therefore, over a length scale of
345 order 50 km, we estimate an Ekman transport convergence, $\frac{\Delta UFe}{\Delta y}$, of $O(10^{-4}) \mu\text{mol m}^{-2} \text{ year}^{-1}$.
346 This is many orders of magnitude smaller than that due to ring-driven transport (Fig. 4), even
347 assuming convergence over a broad area. The dominance of eddies in the lateral transport
348 term agrees with the results from a recently-submitted manuscript based on the results of a
349 $1/10^\circ$ ocean model (Yamamoto A. *et al.*, unpublished data). Diapycnal mixing at the base of

350 the maximum wintertime mixed layer appears to be an extraordinarily small term, since there
351 is a homogenous, low-Fe layer extending all the way to the 1026.75 isopycnal, well beneath
352 the densest subtropical mixed layer (<1026.5). This term scales as $A_v \frac{\Delta Fe}{D}$, where A_v is a
353 turbulent diapycnal diffusivity, typically $O(10^{-5})$, and ΔFe is the vertical iron difference over
354 some depth, D , at the base of the annual maximum mixed layer. Since the vertical Fe
355 gradient is essentially zero near the base of this layer, so too will the turbulent mixing supply
356 be close to zero. Finally, vertical advection is also a small Fe removal term at the base of the
357 annual maximum mixed layer, given the slow downwelling velocities, $O(25 \text{ m year}^{-1})$, acting
358 on the low Fe concentrations 0.3 umol m^3 to yield an estimate for this term of $wFe|_{z=D}$ of -7
359 $\text{umol m}^2 \text{ year}^{-1}$. Hence, the mesoscale eddy-driven supply of Fe and atmospheric deposition
360 appear to far exceed any other physical transport mechanisms. In steady state, the sum of Fe
361 export in organic molecules and other sinking particles should balance these supply terms.

362

363 *Calculation of cross-Gulf Stream phosphate and nitrate fluxes.* Analogous calculations to
364 those for Fe can be made for the ring-driven supply of dissolved phosphate and nitrate, with
365 these calculations advantaged by much greater data coverage. Using GA03 dissolved
366 nutrient data, as well as 7 much higher-resolution sections across the Gulf Stream (6 from the
367 CLIMODE program in January 2006 and February/March 2007^{14,42}, and 1 from cruise
368 EN596 in April 2017 (J. B. Palter, unpublished data), we find that phosphate concentrations
369 just north of the Gulf Stream and above the 1026.5 isopycnal are, on average, 0.2 mmol m^{-3}
370 higher than for the same layer on the subtropical side of the Gulf Stream, whilst for nitrate
371 the corresponding difference is 2.25 mmol m^{-3} . Given the ring characteristics from the
372 altimetry detection and tracking as above, we estimate a ring-driven phosphate supply of
373 $1.3 \times 10^{10} \pm 0.8 \times 10^{10} \text{ mol year}^{-1}$ and a nitrate supply of $14.6 \times 10^{10} \pm 9 \times 10^{10} \text{ mol year}^{-1}$, with
374 uncertainties based on ring statistics as for Fe, and also including variability in phosphate and

375 nitrate concentrations. For comparison, a study using a data-constrained ocean model¹⁸
376 estimated a lateral supply of phosphate plus dissolved organic phosphorus to the North
377 Atlantic subtropical gyre of approximately 3.2×10^{10} mol P year, most of which occurs on the
378 southern fringe of the Gulf Stream. In that coarse-resolution model study, the supply due to
379 lateral mean flow and parameterized eddy mixing was combined into one term that was
380 approximately a factor of 2.5 greater than our estimate for the rings alone, corroborating that
381 rings are likely to provide an important fraction of the total cross-Gulf Stream nutrient
382 supply.

383

384 *Calculation of atmospheric Fe deposition fluxes to the subtropical gyre.* Accurate
385 estimation of soluble Fe flux to the oceans requires knowledge of three parameters: a) aerosol
386 deposition flux; b) Fe content of the deposited aerosols; and c) the fraction of deposited Fe
387 that dissolves in seawater. Whilst the Fe content of mineral aerosol, and Saharan dust in
388 particular, has been shown to be very similar to that of average upper continental crust^{43–46},
389 uncertainties on the other two parameters are large, even leading to disagreement by several
390 orders of magnitude on dust deposition fluxes to the same region⁴⁷. We represent this range
391 in uncertainty by estimating soluble Fe deposition to the NASG using a wide variety of
392 methods, including both extrapolation from observational estimates in the eastern Atlantic
393 close to the Saharan source^{48–50} and at Bermuda in the western Atlantic⁵¹, as well as
394 integration of simulated atmospheric deposition fluxes from numerous modelling studies^{3,52–}
395 ⁵⁷ (Suppl. Info.). The fractional solubility of Fe in atmospheric aerosols ranges from <1% to
396 >95% with a median value of ~3% in the Atlantic Ocean⁵¹. Data compilations as well as
397 studies within the subtropical North Atlantic near Bermuda show that remote marine aerosols
398 have fractional Fe solubility higher than the values of <1% observed for fresh mineral dust,
399 perhaps the result of source composition, natural physical or chemical processing during

400 atmospheric transport, or the increased importance of aerosols from anthropogenic
401 combustion sources^{9,33,51,58,59}. We choose an upper-bound estimate for the solubility of Fe in
402 atmospheric aerosols deposited in the subtropical North Atlantic of 5%, which is among the
403 highest seen in the literature for this region (Suppl. Info.). Thus, our estimate of ring-
404 mediated transport of Fe is compared to what is likely to be a maximum estimate of the
405 atmospheric source. See Suppl. Info. for an extended discussion of all the models and details
406 of the calculations carried out to generate the range described in the main text.

407

408 **References**

409

- 410 1. Gruber, N. & Sarmiento, J. L. Global patterns of marine nitrogen fixation and
411 denitrification. *Global Biogeochem. Cycles* **11**, 235–266 (1997).
- 412 2. Geider, R. J. & La Roche, J. The role of iron in phytoplankton photosynthesis, and the
413 potential for iron-limitation of primary productivity in the sea. *Photosynth. Res.* **39**,
414 275–301 (1994).
- 415 3. Mahowald, N. M. *et al.* Atmospheric global dust cycle and iron inputs to the ocean.
416 *Global Biogeochem. Cycles* **19**, GB4024 (2005).
- 417 4. Conway, T. M. & John, S. G. Quantification of dissolved iron sources to the North
418 Atlantic Ocean. *Nature* **511**, 212–215 (2014).
- 419 5. Sedwick, P. N. *et al.* Iron in the Sargasso Sea (Bermuda Atlantic Time-series Study
420 region) during summer: Eolian imprint, spatiotemporal variability, and ecological
421 implications. *Global Biogeochem. Cycles* **19**, GB4006 (2005).
- 422 6. Boyd, P. W. *et al.* Mesoscale iron enrichment experiments 1993-2005: synthesis and
423 future directions. *Science* **315**, 612–7 (2007).
- 424 7. Moore, C. M. *et al.* Processes and patterns of oceanic nutrient limitation. *Nat. Geosci*
425 **6**, 701–710 (2013).
- 426 8. Tagliabue, A. *et al.* The integral role of iron in ocean biogeochemistry. *Nature* **543**,
427 51–59 (2017).
- 428 9. Jickells, T. D., Baker, A. R. & Chance, R. Atmospheric transport of trace elements and
429 nutrients to the oceans. *Philos. Trans. R. Soc. London A Math. Phys. Eng. Sci.* **374**,
430 20150286 (2016).
- 431 10. Moxim, W. J., Fan, S.-M. & Levy, H. The meteorological nature of variable soluble
432 iron transport and deposition within the North Atlantic Ocean basin. *J. Geophys. Res.*
433 **116**, D03203 (2011).
- 434 11. Moore, C. M. *et al.* Iron limits primary productivity during spring bloom development
435 in the central North Atlantic. *Glob. Chang. Biol.* **12**, 626–634 (2006).
- 436 12. Browning, T. J. *et al.* Iron limitation of microbial phosphorus acquisition in the
437 tropical North Atlantic. *Nat. Commun.* **8**, 15465 (2017).
- 438 13. Olson, D. B. Rings in the Ocean. *Ann. Rev. Earth. Planet. Sci.* **19**, 283-311 (1991).
- 439 14. Palter, J. B., Lozier, M. S., Sarmiento, J. L. & Williams, R. G. The supply of excess

- 440 phosphate across the Gulf Stream and the maintenance of subtropical nitrogen fixation.
 441 *Global Biogeochem. Cycles* **25**, GB4007 (2011).
- 442 15. Williams, R. & MJ, F. The Ekman transfer of nutrients and maintenance of new
 443 production over the North Atlantic. *Deep Sea Res. Pt I.* **45**, 461–489 (1998).
- 444 16. Williams, R. G. *et al.* Nutrient streams in the North Atlantic: Advective pathways of
 445 inorganic and dissolved organic nutrients. *Global Biogeochem. Cycles* **25**, GB4008
 446 (2011).
- 447 17. Williams, R. G., Roussenov, V. & Follows, M. J. Nutrient streams and their induction
 448 into the mixed layer. *Global Biogeochem. Cycles* **20**, GB1016 (2006).
- 449 18. Letscher, R. T., Primeau, F. F. & Moore, J. K. Nutrient budgets in the subtropical
 450 ocean gyres dominated by lateral transport. **9**, 815–819 (2016).
- 451 19. Faghmous, J. H. *et al.* A daily global mesoscale ocean eddy dataset from satellite
 452 altimetry. *Sci. Data* **2**, 150028 (2015).
- 453 20. Mawji, E. *et al.* The GEOTRACES Intermediate Data Product 2014. *Mar. Chem.* **177**,
 454 1–8 (2015).
- 455 21. Jenkins, W. J., Smethie, W. M., Boyle, E. A. & Cutter, G. A. Water mass analysis for
 456 the U.S. GEOTRACES (GA03) North Atlantic sections. *Deep Sea Res. Pt II.* **116**, 6–
 457 20 (2015).
- 458 22. Townsend, D. W. & Ellis, W. G. in *Nutrient Fluxes in Continental Margins: A Global*
 459 *Synthesis* (eds. Liu, K.-K., Atkinson, L., Quinones, R. & Alaue-McManus, L.) 7234–
 460 248 (Springer, 2010).
- 461 23. Palter, J. B., Lozier, M. S. & Barber, R. T. The effect of advection on the nutrient
 462 reservoir in the North Atlantic subtropical gyre. *Nature* **437**, 687–692 (2005).
- 463 24. Rijkenberg, M. J. A. *et al.* The distribution of dissolved iron in the West Atlantic
 464 Ocean. *PLoS One* **9**, e101323 (2014).
- 465 25. Middag, R. *et al.* Intercomparison of dissolved trace elements at the Bermuda Atlantic
 466 Time Series station. *Mar. Chem.* **177**, 476–489 (2015).
- 467 26. Conway, T. M. T. M., John, S. G. S. G. & Lacan, F. Intercomparison of dissolved iron
 468 isotope profiles from reoccupation of three GEOTRACES stations in the Atlantic
 469 Ocean. *Mar. Chem.* **183**, 50–61 (2016).
- 470 27. Wu, J. & Luther, G. W. Spatial and temporal distribution of iron in the surface water
 471 of the northwestern Atlantic Ocean. *Geochim. Cosmochim. Acta* **60**, 2729–2741
 472 (1996).
- 473 28. Conway, T. M. & John, S. G. The cycling of iron, zinc and cadmium in the North East
 474 Pacific Ocean - Insights from stable isotopes. *Geochim. Cosmochim. Acta* **164**, (2015).
- 475 29. Bower, A. S., Rossby, H. T. & Lillibridge, J. L. The Gulf Stream: Barrier or blender?
 476 *J. Phys. Ocean.* **15**, 24–32 (1985).
- 477 30. Qiu, B., Chen, S. & Hacker, P. Effect of mesoscale eddies on subtropical mode water
 478 variability from the Kuroshio Extension System Study (KESS). *J. Phys. Oceanogr.* **37**,
 479 982–1000 (2007).
- 480 31. Lai, D. Y., Richardson, P. L., Lai, D. Y. & Richardson, P. L. Distribution and
 481 Movement of Gulf Stream Rings. *J. Phys. Oceanogr.* **7**, 670–683 (1977).
- 482 32. Buck, K., Sohst, B. M. & Sedwick, P. N. The organic complexation of dissolved iron
 483 along the U.S. GEOTRACES (GA03) North Atlantic Section. *Deep Sea Res. Pt II.*
 484 **116**, 152–165 (2015).
- 485 33. Fishwick, M. P. *et al.* The impact of changing surface ocean conditions on the
 486 dissolution of aerosol iron. *Global Biogeochem. Cycles* **28**, 1235–1250 (2014).
- 487 34. Ward, B. A., Dutkiewicz, S., Moore, C. M. & Follows, M. J. Iron, phosphorus, and
 488 nitrogen supply ratios define the biogeography of nitrogen fixation. *Limnol. Oceanogr.*
 489 **58**, 2059–2075 (2013).

- 490 35. Tilman, D. Resource Competition between Plankton Algae: An Experimental and
491 Theoretical Approach. *Ecology* **58**, 338–348 (1977).
492 36. Deutsch, C., Sarmiento, J. L., Sigman, D. M., Gruber, N. & Dunne, J. P. Spatial
493 coupling of nitrogen inputs and losses in the ocean. *Nature* **445**, 163–167 (2007).
494 37. Twining, B. S. & Baines, S. B. The trace metal composition of marine phytoplankton.
495 *Ann. Rev. Mar. Sci.* **5**, 191–215 (2013).
496 38. Xiu, P., Palacz, A. P., Chai, F., Roy, E. G. & Wells, M. L. Iron flux induced by Haida
497 eddies in the Gulf of Alaska. *Geophys. Res. Lett.* **38**, L13607 (2011).
498

499 Additional Method References

- 500
501 39. Richardson, P. L., Cheney, R. E. & Worthington, L. V. A census of Gulf Stream rings,
502 spring 1975. *J. Geophys. Res.* **83**, 6136 (1978).
503 40. de Boyer Montégut, C., Madec, G., Fischer, A. S., Lazar, A. & Iudicone, D. Mixed
504 layer depth over the global ocean: An examination of profile data and a profile-based
505 climatology. *J. Geophys. Res.* **109**, C12003 (2004).
506 41. LaCasce, J. H. Statistics from Lagrangian observations. *Prog. Oceanogr.* **77**, 1–29
507 (2008).
508 42. The Climode Group. The Climode Field Campaign: Observing the Cycle of
509 Convection and Restratification over the Gulf Stream. *Bull. Am. Meteorol. Soc.* **90**,
510 1337–1350 (2009).
511 43. Trapp, J. M., Millero, F. J. & Prospero, J. M. Trends in the solubility of iron in dust-
512 dominated aerosols in the equatorial Atlantic trade winds: Importance of iron
513 speciation and sources. *Geochemistry, Geophys. Geosystems* **11**, Q03014 (2010).
514 44. Shelley, R. U., Morton, P. & Landing, W. M. Elemental ratios and enrichment factors
515 in aerosols from the US-GEOTRACES North Atlantic transects. *Deep Sea Res. Pt II.*
516 **116**, 262–272 (2015).
517 45. Patey, M. D., Achterberg, E. P., Rijkenberg, M. J. & Pearce, R. Aerosol time-series
518 measurements over the tropical Northeast Atlantic Ocean: Dust sources, elemental
519 composition and mineralogy. *Mar. Chem.* **174**, 103–119 (2015).
520 46. Taylor, S. R. & McLennan, S. M. The continental crust: Its composition and evolution.
521 Blackwell Scientific Publishing (1985).
522 47. Anderson, R. F. *et al.* How well can we quantify dust deposition to the ocean? *Philos.*
523 *Trans. R. Soc. London A Math. Phys. Eng. Sci.* **374**, 20150285 (2016).
524 48. Measures, C. I., Hatta, M., Fitzsimmons, J. N. & Morton, P. Dissolved Al in the zonal
525 N Atlantic section of the US GEOTRACES 2010/2011 cruises and the importance of
526 hydrothermal inputs. *Deep Sea Res. Pt II.* **116**, 176–186 (2015).
527 49. Baker, A. R., Adams, C., Bell, T. G., Jickells, T. D. & Ganzeveld, L. Estimation of
528 atmospheric nutrient inputs to the Atlantic Ocean from 50°N to 50°S based on large-
529 scale field sampling: Iron and other dust-associated elements. *Global Biogeochem.*
530 *Cycles* **27**, 755–767 (2013).
531 50. Powell, C. F. *et al.* Estimation of the Atmospheric Flux of Nutrients and Trace Metals
532 to the Eastern Tropical North Atlantic Ocean. *J. Atmos. Sci.* **72**, 4029–4045 (2015).
533 51. Sholkovitz, E. R., Sedwick, P. N., Church, T. M., Baker, A. R. & Powell, C. F.
534 Fractional solubility of aerosol iron: Synthesis of a global-scale data set. *Geochim.*
535 *Cosmochim. Acta* **89**, 173–189 (2012).
536 52. Luo, C. *et al.* Combustion iron distribution and deposition. *Global Biogeochem. Cycles*
537 **22**, GB1012 (2008).
538 53. Albani, S. *et al.* Paleodust variability since the Last Glacial Maximum and
539 implications for iron inputs to the ocean. *Geophys. Res. Lett.* **43**, 3944–3954 (2016).

- 540 54. Albani, S. *et al.* Improved dust representation in the Community Atmosphere Model.
541 *J. Adv. Model. Earth Syst.* **6**, 541–570 (2014).
542 55. Zhang, Y. *et al.* Modeling the global emission, transport and deposition of trace
543 elements associated with mineral dust. *Biogeosciences Discuss.* **11**, 17491–17541
544 (2015).
545 56. Wang, R. *et al.* Sources, transport and deposition of iron in the global atmosphere.
546 *Atmos. Chem. Phys.* **15**, 6247–6270 (2015).
547 57. Ito, A. & Shi, Z. Delivery of anthropogenic bioavailable iron from mineral dust and
548 combustion aerosols to the ocean. *Atmos. Chem. Phys.* **16**, 85–99 (2016).
549 58. Conway, T. M., Wolff, E. W., Röthlisberger, R., Mulvaney, R. & Elderfield, H. E.
550 Constraints on soluble aerosol iron flux to the Southern Ocean at the Last Glacial
551 Maximum. *Nat. Commun.* **6**, 7850 (2015).
552 59. Longo, A. F. *et al.* Influence of Atmospheric Processes on the Solubility and
553 Composition of Iron in Saharan Dust. *Environ. Sci. Technol.* **50**, 6912–6920 (2016).
554

555 **Acknowledgements**

556

557 We thank all those who contributed to the US GEOTRACES GA03 cruises; the
558 GEOTRACES Program and the Ocean Data Facility who supplied the supporting physical
559 parameters for the USGT11 cruise; Natalie Mahowald, Samuel Albani, Akinori Ito and Rong
560 Wang for making model output available; and Peter Sedwick, Bill Landing, Natalie
561 Mahowald, Chris Measures and Derek Vance for useful discussions. TMC acknowledges
562 support from the University of South Florida; JBP acknowledges support from the University
563 of Rhode Island; GFdS is supported by a Marie Skłodowska-Curie Research Fellowship
564 under EU Horizon2020 (SOSiC, GA #708407).

565

566 **Author Contributions**

567

568 TMC and GFdS conceived the study; JBP carried out the ring-driven Fe transport
569 calculations; GFdS carried out the atmospheric deposition calculations; all authors
570 contributed to the writing of the manuscript.

571

572 **Additional Information**

573

574 Supplementary Information is available in the online version of the paper. Reprints and
575 permissions information is available online at www.nature.com/reprints. Correspondence and
576 requests for materials should be addressed to TMC.

577

578 **Competing Financial Interests**

579 The authors declare no competing financial interests.

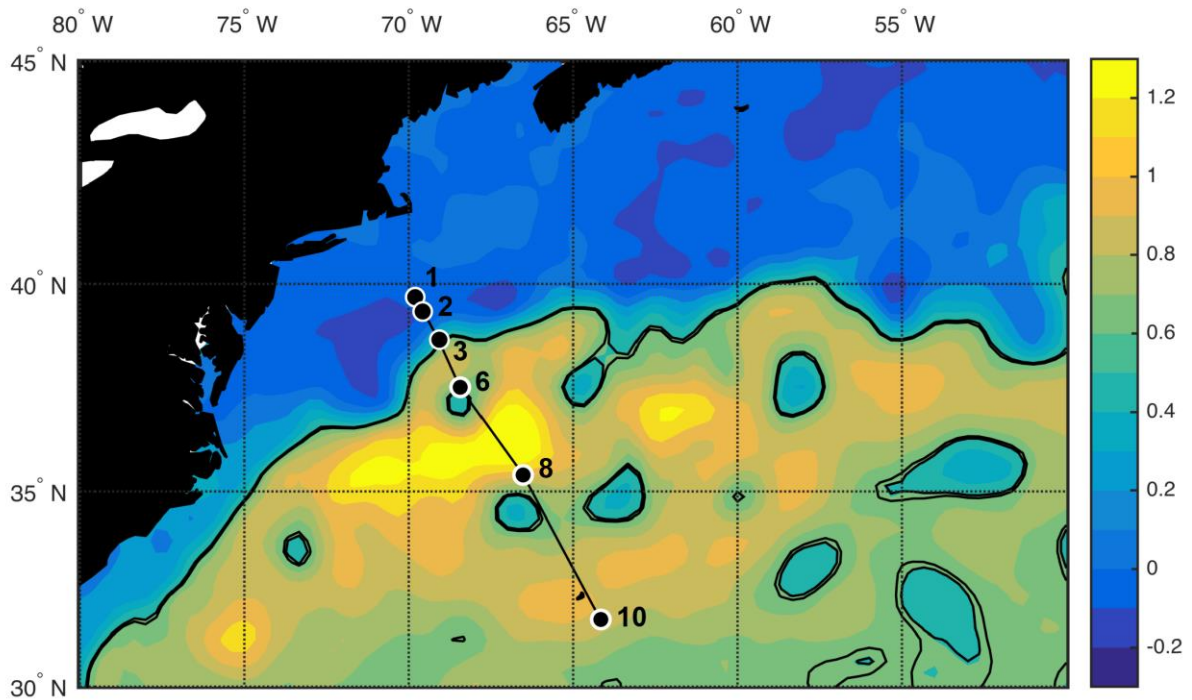


Figure 1. GA03 Fe station sampling locations²⁰, Gulf Stream and cold-core ring in satellite altimetry. Satellite observations of sea-surface height (metres, black contours at 0.52 and 0.55 m) from the AVISO merged mean absolute dynamic topography product (November 9th–16th 2011) show that Station 6, sampled along the GEOTRACES GA03 (USGT11) section (black line) on November 14, 2011, was at the edge of a cold-core ring. Weekly AVISO data shows that the ring was shed from the Gulf Stream between September 28 and October 8, 2011 (see Suppl. Animation 2).

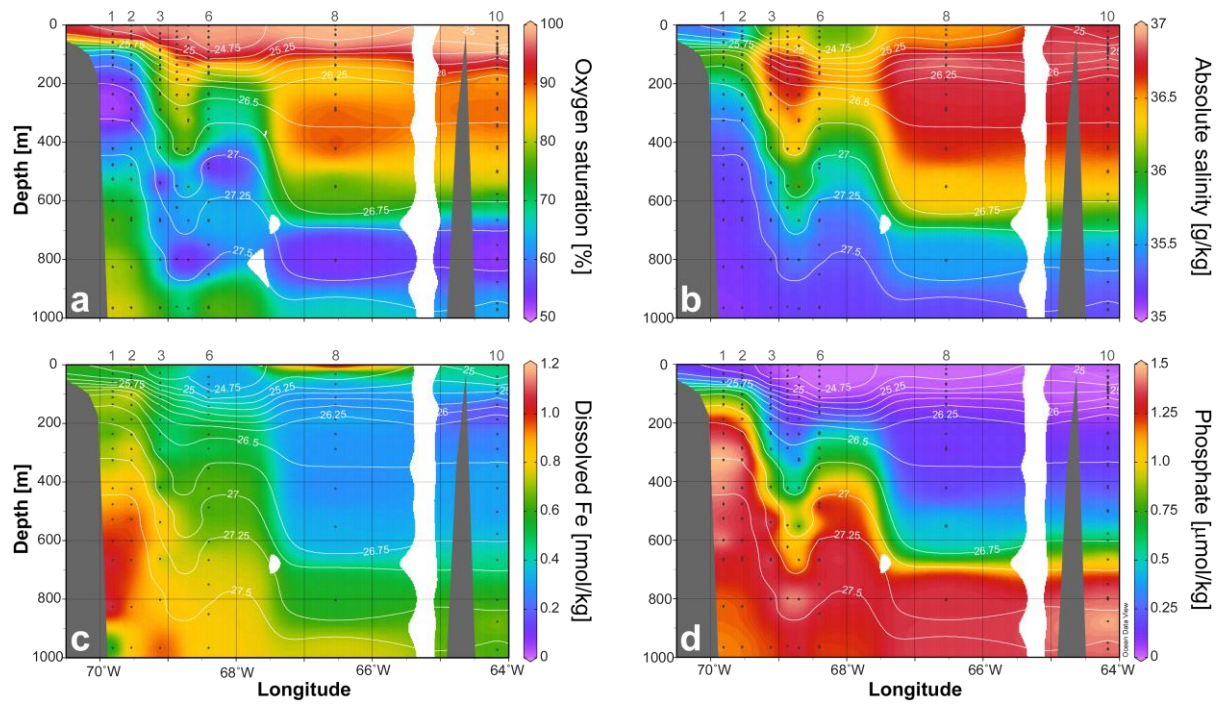
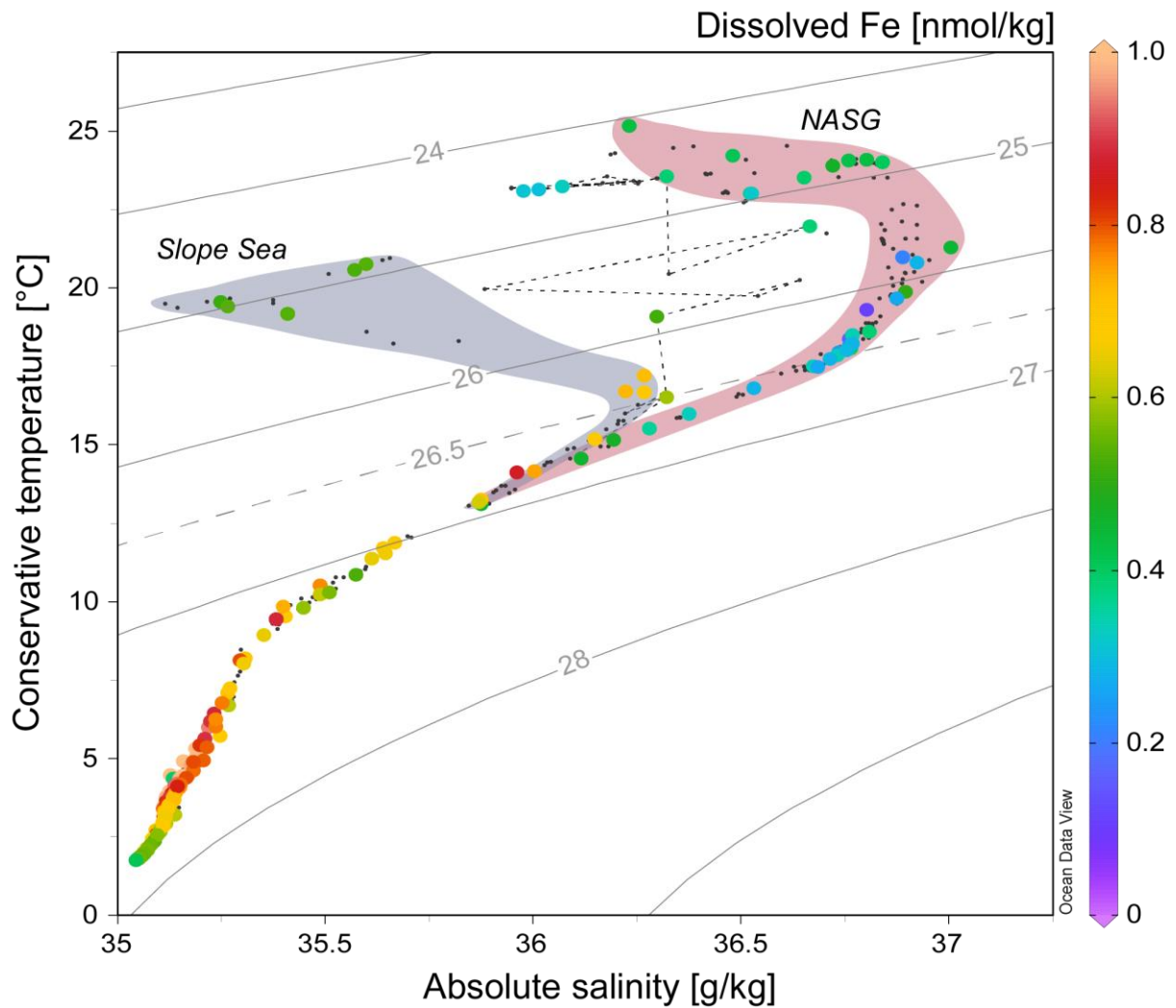
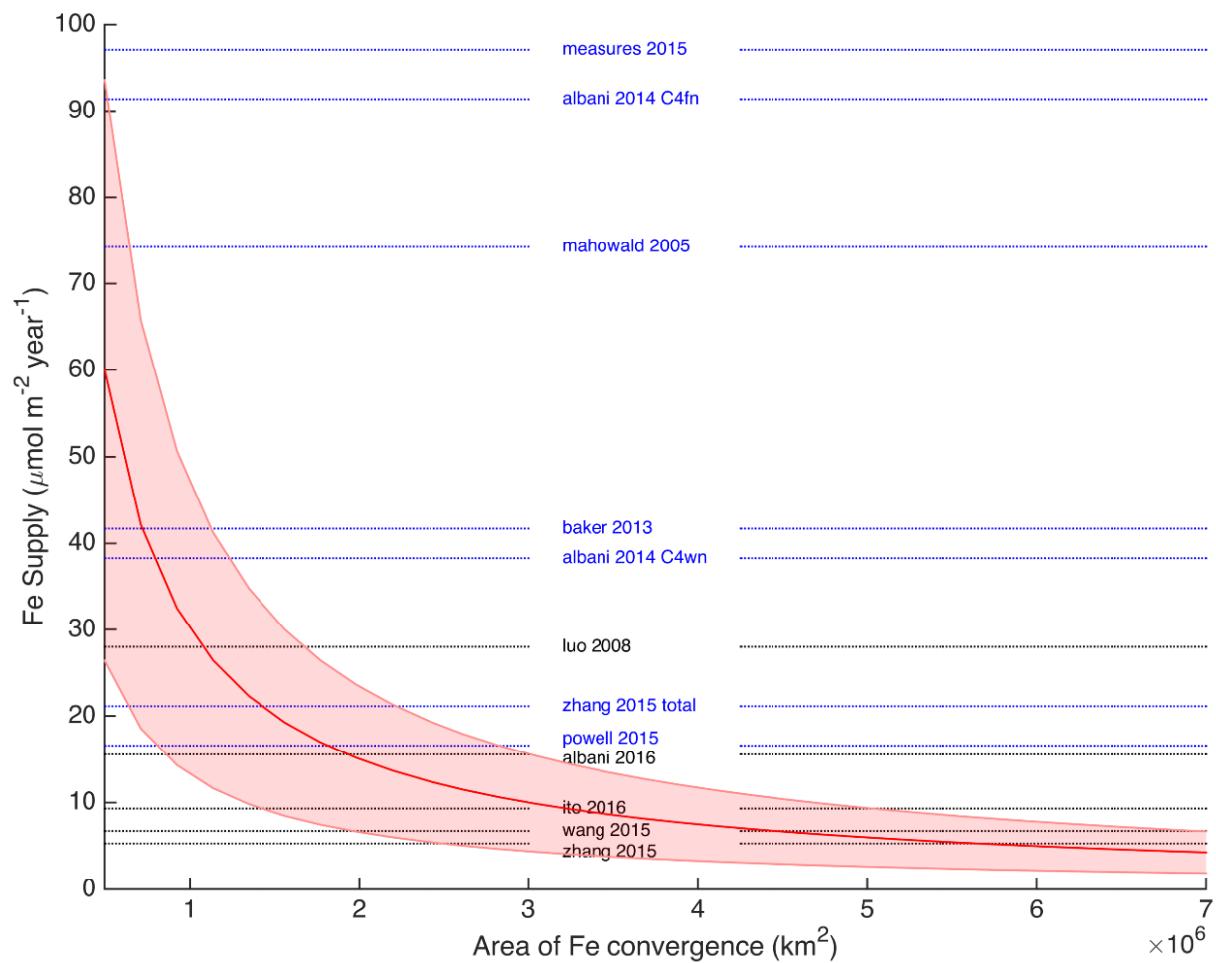


Figure 2. A cold-core ring observed in the GA03 section. The transition from (a) poorly-oxygenated, fresh, Fe- and P-rich waters of the Slope Sea in the west to well-oxygenated, salty, Fe- and P-depleted waters of the gyre^{4,21}. Stations are numbered, and sampling depths marked by dots. To the east of the Gulf Stream (centred around Station 3), the upward doming of isopycnals mark the cold-core ring (Station 6). Two additional stations within the Gulf Stream improve the spatial resolution of oxygen, salinity and phosphate data, which resolve the transition between the gyre and the ring more clearly than the Fe distribution.



580 **Figure 3. GA03 Temperature-salinity diagram, with Fe concentrations⁴ in colour.** The
 581 Slope Sea (grey) has low temperature, low salinity and elevated Fe near the $\sigma_\theta = 26.5$
 582 isopycnal (dashed grey) relative to the NASG (pink). The dashed black line represents
 583 Station 6 at the edge of the ring, with temperature-salinity showing strong interleaving
 584 between the Slope Sea and NASG. Ring Fe concentrations are also elevated, especially
 585 relative to Fe-depleted STMW around the $\sigma_\theta = 26.5$ isopycnal that dominates the subsurface
 586 NASG (Fig. 2). Grey contours show potential density anomaly σ_θ in units of kg m^{-3} .



587 **Figure 4. Ring-driven dissolved Fe supply compared to atmospheric dissolved Fe**
 588 **deposition.** Based on our estimate of total ring-driven Fe supply to the NASG, we calculate
 589 the supply per unit area as a function of the area over which the ring-driven supply converges
 590 (red line; shading denotes uncertainty), ranging from a small region very near the Gulf
 591 Stream to the entire gyre. Horizontal lines show atmospheric deposition of soluble Fe to the
 592 entire NASG from modelling and observational studies. Black lines represent studies that
 593 modelled Fe solubility explicitly, while blue lines represent those to which we applied 5% Fe
 594 solubility (Suppl. Info.).